This is a preprint, the final version is subject to change, of the American Mineralogist (MSA)
Cite as Authors (Year) Title. American Mineralogist, in press.
(DOI will not work until issue is live.) DOI: http://dx.doi.org/10.2138/am-2017-6289

Revision 1

Tourmaline crystal chemistry

FERDINANDO BOSI

Department of Earth Sciences, Sapienza University di Rome, Piazzale Aldo Moro 5, 00185 Rome, Italy

ABSTRACT

Tourmalines form the most important boron rock-forming minerals on Earth. They belong to the cyclosilicates with a structure that may be regarded as a three-dimensional framework of octahedra ZO_6 that encompass columns of structural "islands" made of XO_9, YO_6, BO_3 and TO_4 polyhedra. The overall structure of tourmaline is a result of short-range and long-range constraints depending respectively on the charge and size of ions. In this study, published data are reviewed and analyzed to achieve a synthesis of relevant experimental results and to construct a crystal-chemical model for describing tourmalines and their compositional miscibility over different length scales. Order-disorder substitution reactions involving cations and anions are controlled by short-range structural constraints, whereas order-disorder intracrystalline reaction involving only cations are controlled by long-range structural constraints. The chemical affinity of a certain cation to a specific structural site of the tourmaline structure has been established on the basis of structural data and crystal-chemical considerations. This has direct implications for the tourmaline nomenclature, as well as on petrogenetic and provenance information. Some assumptions behind the classification scheme of tourmaline have been reformulated, revealing major agreement and significant improvements compared to earlier proposed scheme.

Keywords: Tourmaline, order-disorder, crystal structure, nomenclature

INTRODUCTION

The tourmaline supergroup minerals are chemically complex cyclosilicates rich in boron. They are the most common and the earliest boron minerals formed on Earth (Grew et al. 2016). Tourmalines are widespread in Earth's crust, typically occurring in granites and granitic pegmatites but also in sedimentary and metamorphic rocks (Dutrow and Henry 2011; van Hinsberg et al. 2011). In recent years it was demonstrated that tourmalines preserve important records of the geological conditions in which they form in the lithosphere, thus it is important that we can understand how to read those records (e.g., Dutrow and Henry 2011). The general formula may be written as: $XY_3Z_6T_6O_{18}(BO_3)_3V_3W$, with X = Na^+, K^+, Ca^{2+}, □ (= vacancy); Y = Al^{3+}, Cr^{3+}, V^{3+}, $Fe^{2+/3+}$, Mg^{2+}, Mn^{2+}, Li^+, Ti^{4+}; Z = Al^{3+}, Cr^{3+}, V^{3+}, $Fe^{2+/3+}$, Mg^{2+}; T = Si^{4+}, Al^{3+}, B^{3+}; B = B^{3+}, V = $(OH)^-$, O^{2-}; W = $(OH)^-$, F^-, O^{2-} being the most common constituents. The letters in the formula (X, Y, Z, T and B, not italicized) represent groups of cations at the $^{[9]}X$, $^{[6]}Y$, $^{[6]}Z$, $^{[4]}T$ and $^{[3]}B$ crystallographic sites (letters italicized). The letters V and W represent groups of anions at the $^{[3]}$O3 and $^{[3]}$O1 sites, respectively. The H atoms occupy the H3 and H1 sites which are related to O3 and O1, respectively.

Since the publication of the nomenclature of the tourmaline-supergroup minerals (Henry et al. 2011), several new members of tourmaline have been approved by the Commission on New Minerals, Nomenclature and Classification (CNMNC) of the International Mineralogical Association (IMA). These include oxy-species characterized by high contents of Al^{3+}, Cr^{3+}, V^{3+} and $Fe^{2+/3+}$, which have provided a better understanding of the tourmaline crystal chemistry. This paper will present a general picture of the tourmaline structure and crystal chemistry, showing major factors controlling stability and chemical constraints from a short- and long-range structural viewpoint. The critical recognition of the importance of charge and size of atoms in determining

crystal-chemical properties and miscibility behavior will be emphasized as well as critical comments on the assumptions behind the classification scheme of tourmaline. The importance of the crystal-chemical control of the tourmaline composition has direct implications on nomenclature as well as on the petrogenetic and provenance information (e.g., Hawthorne and Henry 1999).

TOURMALINE CONSTITUENTS AND SPECIES

The compositional range of tourmaline is remarkable, including important constituents with more than one oxidation state (e.g., Fe^{2+}-Fe^{3+} and Mn^{2+}-Mn^{3+}) and other characterizing synthetic tourmalines (e.g., Ag^{+}, Co^{2+}, Ni^{2+}, Cu^{2+} and Ga^{3+}; London et al. 2006; Rozhdestvenskaya et al. 2012; Vereshchagin et al. 2013, 2015, 2016). A total of (at least) 26 relevant constituents, in terms of concentration or occurrence, have been unambiguity identified in tourmaline (Table 1). These constituents are very different in charge and size and accommodate into seven crystallographic sites (*X*, *Y*, *Z*, *T*, *B*, O1 and O3); the other sites (O2, O4, O5, O6, O7 and O8) are solely occupied by oxygen. Moreover, the number of constituent-coordination environments is relatively large, compared to most other minerals: [3], [4], [6] and [9] coordination. Thus, tourmaline violates the Pauling's parsimony rule, which emphasizes that the number of topochemically different environments in a structure tends to be small (Hawthorne 2006). In theory, this relatively large number of substantially different sites would decrease the stability, but tourmaline exists over environments that extend from the surface of the crust to the upper mantle (e.g., Marschall et al. 2009; Lussier et al. 2016) in the presence of H_2O, B- and F-bearing fluids.

The dominance of tourmaline constituents at one or more sites of the structure gives rise to a range of mineral species. At present, the tourmaline supergroup consists of 33 mineral species approved by the IMA-CNMNC (Table 2).

CRYSTAL STRUCTURE

The tourmaline structure is typically rhombohedral, space-group $R3m$ with $Z = 3$, although some studies report lower symmetry such as orthorhombic, monoclinic or triclinic (e.g., Akizuki et al. 2001; Shtukenberg et al. 2007; Hughes et al. 2011). Tourmaline has an intermediate structural complexity of about 200 bits per unit cell (Krivovichev 2013), which is larger than that of amphibole (about 150 bits per unit cell), but smaller than that of some other minerals such as analcime (usually much over 200 bits per unit cell).

The tourmaline structure may be regarded as one of the most elegant of all crystal structures. It belongs to the subclass of cyclosilicate as consists of rings of six TO_4 tetrahedra, lying in a plane parallel to (0001). Because all tetrahedra point in the same direction, tourmaline lacks center symmetry (polar character) and is both pyroelectric and piezoelectric (electrical properties). Each tetrahedron shares one edge with the trigonal antiprism XO_9, which is located along the 3-fold axis passing through the center of each six-membered ring [T_6O_{18}]. The X-site occupancy usually reflects the paragenesis of the rock in which tourmaline crystallizes (petrologic information), and tourmaline supergroup is classified into primary groups based on the dominant occupancy of the X site: vacant, alkali and calcic groups (Henry et al. 2011). The antiprism XO_9 and the ring [T_6O_{18}] combine with two sets of three octahedra YO_6: an [Y_3O_{15}] triplet of octahedra caps the XO_9 polyhedron toward the +**c** axis and the other [Y_3O_{13}] caps the [T_6O_{18}] ring of tetrahedra toward the –**c** axis. The most extensive compositional variation occurs at the Y site, which is able to incorporate constituents of different sizes and charges (including vacancies) that makes tourmaline famous for its extensive range of colors (all rainbow colors) even within individual crystals (oscillatory and sector zoning). The BO_3 groups oriented sub-parallel to (0001) lie between the tetrahedral rings and are fully occupied by B, which makes tourmaline one of the most important B-bearing minerals (reservoir of B) in the Earth. The structural arrangement of [T_6O_{18}], XO_9, [Y_6O_{18}] and $(BO_3)_3$ form "islands" that are stacked in columns along the **c** axis. These islands are attached to one another

along the **a** and **b** crystallographic axes by spiral chains of ZO_6 octahedra (Fig. 1), which also extend along to the **c** axis according to a 3_1 triad screw axis. The three-dimensional framework of the tourmaline structure is therefore given by the screw-like arrangement of ZO_6 (Fig. 2). This framework is characterized by similar strong *Z*-O bonds (~ 0.5 valence units) which would explain some physical properties: hardness (~ 7-7½ Mohs), lack of cleavage, resistance to weathering in clastic sediments (like rutile and zircon), and extensive pressure-temperature stability up to about 7 GPa and 950 °C. Finally, another important feature of the tourmaline structure is provided by the orientation of the hydrogen atoms, which are sub-parallel to the **c** axis: H1-hydrogen point down –**c** towards the oxygen at O1, and H3-hydrogen points up +**c** towards the oxygen at O3. Owing to this orientation of (OH) dipoles, the fundamental (OH)-stretching bands in infrared spectra of tourmalines will display a very strong pleochroism, with $\varepsilon >> \omega$ (e.g., Skogby et al. 2012). All polyhedra discussed above are distorted. With respect to the ideal volume, bond distance or bond angle, the distortion of polyhedra decrease with decreasing coordination number according to the sequence: $XO_9 > YO_6 > ZO_6 > TO_4 > BO_3$ (Ertl et al. 2002; Bosi and Lucchesi 2007).

In summary, the tourmaline structure may be considered as a three-dimensional framework of octahedra ZO_6 that must be able to accommodate the structural islands.

STRUCTURAL CONSTRAINTS

Henry and Dutrow (2011) showed that the accommodation of F at the O1 site is influenced by the cation occupancy (total charge) of the *X* and the *Y* sites. They suggested that the manner in which chemical constituents are incorporated into the tourmaline structure depends on external influences (temperature, pressure, mineral local assemblages and fluid composition) and on internal influences (crystallographic constraints). Moreover, tourmaline may be extremely optically, chemically, and isotopically zoned due to the occurrence of extensive short-range order of atoms

that may strongly decrease the diffusion rates of atoms in the structure (e.g., Hawthorne and Dirlam 2011).

In general, the tourmaline chemical composition and zoning is a result of external and internal constraints. The latter act from a scale of a few Å (short-range structure) to a scale that involve the complete crystal (long-range structure).

Short-range structure

Short-range structure involves a set of atoms (cluster) that do not obey to the translational symmetry. Each cluster is controlled by bond-valence requirements, i.e., the charge of ions needs to be neutralized locally by nearest neighbors. Of particular relevance for tourmaline are the local atomic arrangements around the O1 (bonded to 3*Y*) and O3 (bonded to *Y*+2*Z*) sites which show a greater chemical variability. Hawthorne (1996; 2002) and Bosi (2010; 2011; 2013) evaluated possible atomic arrangements around O1 and O3, constrained by the valence-sum rule. According to the Bond Valence Model (e.g., Brown 2016), there is a tendency for the sum of the bond valences (BVS) around each atom to approach its formal valence (FV); if a large mismatches between BVS and FV occur, it is indicative of strained bonds which lead to instability in the structure. As a result, those local arrangements that most closely conform to the valence-sum rule are the arrangements that are most likely to occur in the structure (Hawthorne et al. 2005; Hawthorne 2016). The allowed stable short-range arrangements expressed as charge arrangements around O1 and O3 of tourmaline are summarized in Table 3. These arrangements can be considered as short-range constraints and have significant effects on the chemistry of short-range structure. For example, in oxy-foitite, ideally $\square^{Y}(Fe^{2+}Al_2)^{Z}(Al_6)(Si_6O_{18})(BO_3)_3{}^{O3}(OH)_3{}^{O1}(O)$, the *Y* and O1 sites composition would require the short-range arrangement $^{Y}(Fe^{2+} + 2Al)\text{-}^{O1}(O^{2-})$ rather than the chemically equivalent proportion of 33% $^{Y}(3Fe^{2+})\text{-}\ ^{O1}(O^{2-})$ plus 67% $^{Y}(3Al)\text{-}\ ^{O1}(O^{2-})$, because the arrangement $^{Y}(3Fe^{2+})\text{-}\ ^{O1}(O^{2-})$ is unstable from a bond valence perspective. Similarly, the *Y*, *Z* and O3 sites composition

requires specific proportions of short-range arrangements, 33% $[^{Y}Fe^{2+} + {}^{Z}(2Al)]\text{-}{}^{O3}(OH)$ plus 67% $[^{Y}Al + {}^{Z}(2Al)]\text{-}{}^{O3}(OH)$.

Therefore, the short-range constraints will tend to favor specific cation arrangements around the anions at the O1 and O3 sites. We can also note that the local arrangements around O^{2-} of Table 3 can be associated with occupants having a total charge higher than that of occupants around (OH,F). This is consistent with the study of Bosi (2013), who examined the bond valences of a large number of refined tourmaline structures and showed a well-developed linear correlation between BVS at the O1 site and MFV (mean formal valence = total charge divided by the site multiplicity) at the *Y* site: BVS(O1) = 0.99 · MFV(*Y*) – 1.20 (see also Fig. 1 of Bosi 2013). Such a correlation indicates that $^{O1}O^{2-}$ content increases with increasing of $^{Y}R^{3+}$content as suggested by Table 3, and may hence be considered as the linking between what predicted by bond valence arguments in the short-range structure with what observed by the diffraction techniques in the long-range structure.

As the sum of all different stable short-range arrangements corresponds to occupancies of the sites averaged over the complete crystal, it is apparent that (i) the stable short-range structures affects the long-range structure, (ii) the short-range constraints may have significant effects on the variation in chemical composition of tourmalines such as atomic substitutions and order-disorder mechanisms. In this regard, consider that the relation between dravite and oxy-dravite can be formulated by the chemical substitution:

$$Mg^{2+} + (OH)^{-} \leftrightarrow Al^{3+} + O^{2-}$$

corresponding to the order-disorder mechanism

$$[^{Y}(3Mg^{2+}) + {}^{O1}(OH)^{-}] + {}^{Z}Al^{3+} \leftrightarrow [^{Y}(2Al^{3+} + Mg^{2+}) + {}^{O1}(O^{2-})] + {}^{Z}Mg^{2+}$$

This mechanism involves the stable short-range arrangements $[^{Y}(3R^{2+})\text{-}{}^{O1}(OH)]$ and $[^{Y}(2R^{3+} + R^{2+})\text{-}{}^{O1}(O)]$ compatible respectively with dravite and oxy-dravite (or maruyamaite), and it can be

simplified to $2^{Y}Mg^{2+} + {}^{O1}(OH)^{-} + {}^{Z}Al^{3+} \leftrightarrow 2^{Y}Al^{3+} + {}^{O1}(O^{2-}) + {}^{Z}Mg^{2+}$ (Hawthorne 1996). Similarly, dravite and povondraite are related by the chemical substitution:

$$Mg^{2+} + 6Al + (OH)^{1-} \leftrightarrow 7Fe^{3+} + O^{2-}$$

corresponding to the order-disorder mechanism

$$[{}^{Y}(3Mg^{2+}) + {}^{O1}(OH)^{-}] + 6{}^{Z}Al^{3+} \leftrightarrow [{}^{Y}(3Fe^{3+}) + {}^{O1}(O^{2-})] + 2{}^{Z}Mg^{2+} + 4{}^{Z}Fe^{3+}$$

This mechanism involves the stable short-range arrangements $[{}^{Y}(3R^{2+})\text{-}{}^{O1}(OH)]$ and $[{}^{Y}(3R^{3+})\text{-}{}^{O1}(O)]$ compatible with dravite and povondraite, respectively.

The two mechanisms reported above can be generalized to:

$$2^{Y}R^{2+} + {}^{Z}R^{3+} + {}^{O1}(OH,F)^{1-} \leftrightarrow 2^{Y}R^{3+} + {}^{Z}R^{2+} + {}^{O1}(O^{2-}) \quad (1)$$

$$3^{Y}R^{2+} + 2^{Z}R^{3+} + {}^{O1}(OH,F)^{1-} \leftrightarrow 3^{Y}R^{3+} + 2^{Z}R^{2+} + {}^{O1}(O^{2-}) \quad (2)$$

which are actually order-disorder *substitution* reactions involving cations and anions and controlled by local bond-valence requirements at the O1 site, i.e., short-range constraints.

Besides order-disorder *substitution* reactions (1) and (2), there is another type of order-disorder reaction that involves only cations:

$${}^{Y}R^{3+} + {}^{Z}R^{2+} \leftrightarrow {}^{Y}R^{2+} + {}^{Z}R^{3+} \quad (3)$$

The latter is an intracrystalline reaction usually controlled by long-range constraints (see below).

Long-range structure

The short-range constraints control which atoms can be nearest neighbors and hence determine the short-range structure. The sum of all of the short-range arrangements leads to a long-range structure. The latter is determined mainly by spatial/steric constraints (imposed by translational symmetry) that restrict the number of ways in which ions can be bonded to each other in the three-dimensional space. For a long-range structure to be formed, both short-range and long-range constraints must be satisfied. Consequently, all involved short-range arrangements need to be consistent with geometrical requirements, that is, with specific long-range interatomic distances.

In tourmaline, the three-dimensional framework of the ZO_6 polyhedra must be able to accommodate the structural islands (Fig. 2). On the basis of 127 structure refinement (SREF) data, Bosi and Lucchesi (2007) presented a structural stability field for tourmaline as a function of <*Y*-O> and <*Z*-O>, suggesting that only a limited mismatch in the dimensions between <*Y*-O> and <*Z*-O> can be tolerated by the structure. At present, additional SREF can be found in the literature (at least 195, for a total of 322 data sets), which confirm the occurrence of a dimensional difference Δ_{Y-Z} = <*Y*-O> – <*Z*-O> in the range between 0.00 Å and 0.15 Å (Fig. 3). All known tourmalines fall within the delineated field indicating the presence of a long-range structural constraint. As values outside the range 0.00-0.15 Å have never been correctly observed so far, possible anomalous data need to be carefully checked: for example, the mean bond distances of lucchesiite from Czech Republic (Bosi et al. 2017a), <*Y*-O> = 2.095 Å and <*Z*-O> = 1.932 Å, yielded Δ_{Y-Z} = 0.16 Å (> 0.15 Å). However, a careful check of the *Y*-O distances showed a mistake in the calculation of <*Y*-O>. The correct value is actually 2.065 Å which is fully consistent with the empirical structural constraint mentioned above: Δ_{Y-Z} = 0.13 Å (< 0.15 Å).

The stability field <*Z*-O> versus <*Y*-O> also describes and predicts the effects of the tourmaline structural stability on its chemical variability. For instance, Bosi and Lucchesi (2007) predicted that the end-member compositions of dravite, schorl and tsilaisite (i.e., species with the *Y* site occupied by R^{2+}-cations and the *Z* site occupied by Al) should never occur, neither as natural samples nor as synthetic samples, because their structures should be unstable: $<^{Y}Mg\text{-}O>$, $<^{Y}Fe^{2+}\text{-}O>$ and $<^{Y}Mn^{2+}\text{-}O>$ distances are too large with respect to $<^{Z}Al\text{-}O>$. In this regard, the case of fluor-dravite (an oxy-*free* species) nicely illustrates the effect of long-range constraint on tourmaline site populations. According to the chemical analysis (Clark et al. 2011), the structural formula of fluor-dravite is expected as follows: $Na^{Y}(Mg_2Fe^{2+})^{Z}(Al_6)(Si_6O_{18})(BO_3)_3(OH)_3{}^{O1}[F_{0.7}(OH)_{0.3}]$, with expected <*Y*-O> ~ 2.100 Å and <*Z*-O> ~ 1.907 Å, derived from the ionic radii (see below). These expected distances yield Δ_{Y-Z} = 0.19 Å > 0.15 Å, indicating that the fluor-dravite structure is

unstable. However, SREF data clearly show that the observed <*Y*-O> = 2.053 Å and <*Z*-O> = 1.913 Å are consistent with the long-range constraint (Δ_{Y-Z} = 0.14 Å < 0.15 Å) because the *Y* and *Z* site population is actually disordered: …$^{Y}(Mg_{1.4}Al_{0.6}Fe^{2+}_{1.0})_{\Sigma 3.0}$ $^{Z}(Al_{5.4}Mg_{0.6})_{\Sigma 6.0}$… (Clark et al. 2011). In fact, the intracrystalline order-disorder reaction $^{Y}Al^{3+} + {}^{Z}Mg^{2+} \leftrightarrow {}^{Y}Mg^{2+} + {}^{Z}Al^{3+}$, not involving anions, occurs to shorten <*Y*-O> (by introducing Al^{3+}) and to enlarge <*Z*-O> (by introducing Mg^{2+}), thus to accommodate the potential misfit between $^{Y}MgO_6$ and $^{Z}AlO_6$.

In summary, the tourmaline structure is a result of short-range constraints depending on the charge of ions, and long-range constraints depending on the size of ions. Order-disorder substitution reactions such as (1) and (2) involve cations and anions and are controlled by the short-range constraints, whereas order-disorder (usually) intracrystalline reaction (3) involves only cations and are controlled by the long-range constraints.

THE IONIC RADII

Variations in mean bond distances are often encountered in mineral crystal structures. In accordance with the Bond Valence Model, these variations may be explained as function of the degree of strain occurring in coordination environments of cations (Bosi 2014). In line with the mineralogical convention, any variation in mean bond distance is expressed as a variation in the cation radius by keeping the anion radius fixed, although the oxide anion radius can show a wide range of values (e.g., Gibbs et al. 2014).

Bosi and Lucchesi (2007) refined empirical ionic radii for six-fold coordinated ions in tourmaline and showed that the $^{[6]}$Al ionic radius varies in a range of values larger than the expected one: the observed variation of $<^{Z}$Al-O>, 1.900-1.912 Å with a grand mean value 1.906 Å (Fig. 3 of Bosi and Andreozzi 2013), is larger than 1.892 Å calculated from Shannon (1976). A significant size variation was also reported for the $^{[6]}Fe^{3+}$ ionic radius (0.645-0.705 Å) as well as for the other ions depending on the *Y* or *Z* site occupancy. The reasons of these variations may be ascribed to

248 experimental errors (e.g., Bosi and Andreozzi 2013), inductive effects from other parts of the
249 structure (e.g., Ertl et al. 2012a), different occupancies at the octahedrally coordinated sites (e.g.,
250 Bosi and Lucchesi 2007), or more generally to different degree of strain experienced by atoms in
251 the bonding environment (Bosi 2014).

252 Although the *Y* and *Z* ionic radii of Bosi and Lucchesi (2007) fitted with 93% of the *Y* and *Z*
253 mean bond distances analyzed, their size variations are of little practical interest for crystal-
254 chemical considerations. It is convenient to report such ionic radii by a unique mean value with its
255 standard error (±σ). The latter can be estimated as the difference between the maximum and
256 minimum radius reported in Table 2 of Bosi and Lucchesi (2007) divided by 4 or from the above
257 mentioned distance variations for Al: $2\sigma_{Al} = \pm (1.912 - 1.900)/2 = \pm 0.006$ Å, then $\sigma_{Al} = \pm 0.003$ Å.
258 Table 4 shows such mean ionic radii for [6]-coordinated ions in tourmaline.
259

260 ## CATION SITE PREFERENCE FOR *Y* AND *Z*

261 Because <*Y*-O> is always greater than <*Z*-O> in tourmaline, the *Y* site will tend to
262 incorporate relatively large cations, whereas the *Z* site will tend to incorporate relatively small
263 cations. Moreover, the chemical affinity of a certain cation to a specific structural site of the
264 tourmaline structure can be established on the basis of structural data and crystal-chemical
265 considerations. Bosi et al. (2017b) proposed that the preference of R^{3+}-cations for the *Y* and *Z* sites
266 is mainly controlled by their ionic radius according to the sequence: $^{Y}V^{3+} > {}^{Y}Cr > {}^{Y}Al$ and $^{Z}Al > {}^{Z}Cr$
267 $> {}^{Z}V^{3+}$. This conclusion is consistent with the cation distributions over *Y* and *Z* observed for the
268 oxy-species such as vanadio-oxy-chromium-dravite, vanadio-oxy-dravite and chromo-alumino-
269 povondraite (Table 2) as well as with the fact that no tourmaline species with atomic arrangements
270 such as "…$^{Y}(Al,Cr)_3{}^{Z}(Mg_2V_4)$…" have been documented so far. Ferric iron can also be included in
271 this sequence on the basis of the Fe^{3+}-Al crystal-chemical behavior in bosiite,

"…$^{Y}(Fe^{3+})_3{}^{Z}(Mg_2Al_4)$…" (Ertl et al. 2016), and the relatively large ionic radius of Fe^{3+}. Therefore, the preference for the R^{3+}-cations to occupy the *Y* and *Z* sites is of type:

$$^{Y}Fe^{3+} > {}^{Y}V^{3+} > {}^{Y}Cr^{3+} > {}^{Y}Al^{3+}$$

$$^{Z}Al^{3+} > {}^{Z}Cr^{3+} > {}^{Z}V^{3+} > {}^{Z}Fe^{3+}$$

Similar arguments apply to the R^{2+}-cations (Bosi and Skogby 2013; Bosi et al. 2015a; Vereshchagin et al. 2015): the preference of R^{2+} for the *Z* site increases with decreasing ionic radius. An opposite preference is expected for the *Y* site. Therefore, the preference for the R^{2+}-cations to occupy the *Y* and *Z* sites is of type:

$$^{Y}Mn^{2+} > {}^{Y}Fe^{2+} > {}^{Y}Co^{2+} > {}^{Y}Mg^{2+} > {}^{Y}Ni^{2+}$$

$$^{Z}Ni^{2+} > {}^{Z}Mg^{2+} > {}^{Z}Co^{2+} > {}^{Z}Fe^{2+} > {}^{Z}Mn^{2+}$$

On the degree of R^{2+}-R^{3+} order-disorder over the *Y* and *Z* sites

In minerals, cation substitutions in a structural site are usually controlled by ion sizes (Goldschmidt's rules). In this regard, the cation-size mismatch is a useful parameter to predict the extension of chemical substitution series: size difference between ions less than ~15% indicates a wide substitution; by ~15 to ~30% indicates a partial substitution; more than ~30% indicates little substitution.

In tourmaline, the cation-size mismatch can explain the amount of R^{2+} replacing R^{3+} at the *Z* site, which occurs in the chemical reactions (1), (2) and (3). Using the ionic radii of Table 4, the difference in size between Al^{3+} and R^{2+}-cations are: Al-Ni^{2+} ~ 21%, Al-Mg^{2+} ~ 24%, Al-Co^{2+} ~ 27%, Al-Fe^{2+} ~ 30% and Al-Mn^{2+} ~ 32%. These values suggest the occurrence of a partial and little substitution between ^{Z}Al and $^{Z}R^{2+}$-cations. The negative correlation between Al-R^{2+} cation-size mismatch and the maximum $^{Z}R^{2+}$-occupancy observed for tourmalines with Al > 5 apfu, strongly supports the dependence of ionic radius on substitution degree (Fig. 4). Similarly, the different crystal-chemical behavior of ^{Z}Mg observed in Cr- and Al-oxy-tourmalines can be explained. As

297 difference in size Cr^{3+}-Mg^{2+} (~15%) is smaller than Al-Mg^{2+} (~24%), the ^{Z}Mg content in Cr-oxy-
298 tourmalines is expected to be larger than that in Al-oxy-tourmalines. This is confirmed by the site
299 populations of oxy-chromium-dravite and oxy-dravite (or maruyamaite): "…$^{Y}(Cr)_3{}^{Z}(Mg_2Cr_4)$…"
300 and "…$^{Y}(MgAl_2)^{Z}(MgAl_5)$…", respectively (Bosi et al. 2012; Bosi and Skogby 2013; Lussier et al.
301 2016).
302

303 ## NOMENCLATURE ISSUES

304 Tourmaline site occupancies depend essentially on the charge and size of atoms forming
305 specific arrangements that obey both the short-range and long-range structural constraints. This
306 crystal-chemical control of tourmaline composition should be reflected in systematic procedure for
307 classification.

308 The tourmaline nomenclature is based on the determination of the chemical content at each
309 non-equivalent site of the crystal structure (Hawthorne and Henry 1999). Consequently, a structural
310 formula $XY_3Z_6T_6O_{18}(BO_3)_3V_3W$ is required for classification purposes. In accordance with the
311 IMA-CNMNC guidelines (e.g., Nickel and Grice 1998; Hatert and Burke 2008), this means that the
312 chemical information of the *Y* and *Z* site should not be merged, because such sites have different
313 crystal-chemical response to the atom accommodations. For identifying tourmaline species, Henry
314 et al. (2011, 2013) pointed out the importance of the *empirical structural formula* stating that the
315 "actual tourmaline structural information of the *Y*- and *Z*-site occupancy is an overriding
316 consideration for the definition of a tourmaline species".

317 Only in absence of specific structural information on *Y* and Z occupancy, Henry et al. (2013)
318 recommended the following site allocation procedure for the *Z* and *Y* sites: "Initially assign all Al
319 (in excess of that assigned to the *T* site) to the *Z* site. Next, successively assign Mg^{2+} (up to 2 apfu),
320 V^{3+}, Cr^{3+}, and Fe^{3+}. If there is an excess of trivalent cations on the Z site, the excess trivalent cations
321 go into the *Y* site". As a result, tourmaline species can also be classified by combining chemical

data with assumptions on the site allocation of atoms, which lead to a *calculated structural formula*. However, the application of such nomenclature rules results in ambiguity for identifying oxy-tourmalines.

Table 5 shows that the empirical and calculated structural formulae of selected oxy-tourmaline species do not converge to same mineral name. In detail, sample PR1973 and TM84a can be only identified by the empirical structural formula. Sample PR85m is identified as oxy-schorl by the empirical formula and as oxy-dravite by the calculated formula. Sample drv18 is quite anomalous as both its empirical and its calculated formula lead to two new end-member formulae: $Na(Mg_2Fe^{3+})Al_6Si_6O_{18}(BO_3)_3(OH)_3O$ and $Na(Fe^{2+}{}_2Fe^{3+})Al_6Si_6O_{18}(BO_3)_3(OH)_3O$, respectively. These formulae, however, appear to represent an unresolved issue in the classification scheme rather than the occurrence of new species.

The unsuccessful application of the procedure of Henry et al. (2013) for naming tourmaline species may be ascribed to inaccurately developed cation site distributions, concerning in particular (i) the incorrect site preference of V^{3+} and Cr^{3+} for the *Z* site, which should be reversed as first $^{Z}Cr^{3+}$ and then $^{Z}V^{3+}$ (see above), and (ii) the assumed qualitative Al site distribution, which incorrectly increases the actual amount of Al at the *Z* site. In order to improve this procedure, the site partitioning of important cations such as Al should be correctly modelled. Of particular relevance in this regard is the plot of ^{Z}Al versus $^{[6]}Al$ (= $Al_{tot} - {}^{T}Al$), obtained using cation-distribution data of 83 oxy-tourmalines accompanied by SREF, showing a strong positive nonlinear relation (Fig. 5). In detail, the plot displays the occurrence of an almost linear trend with $^{Z}Al/^{[6]}Al$ ratio very close to 1 for $^{[6]}Al < 4$ apfu, and a nonlinear trend for $^{[6]}Al > 4$ apfu. In order to make prediction from experimental data, the following quadratic equation may be used:

$$^{Z}Al = -0.1155 + 1.1713 \cdot {}^{[6]}Al - 0.0522 \cdot {}^{[6]}Al^2 \quad (4)$$

Equation (4) allows assigning amounts of Al at the *Z* site using only chemical data. Notice that this quadratic fitting does lead to non-physical values for extrapolated values of $^{[6]}Al$ ranging from

0.000 to 0.098 apfu (^{Z}Al assumes slightly negative values) and from 8.270 to 9.000 apfu (^{Z}Al assumes values slightly larger than 6.000 apfu). An empirical site assignment model could also be attained for Mg, but the correlation of ^{Z}Mg versus $^{[6]}Al_{tot}$ (not shown) is not yet sufficiently accurate to make prediction. Similarly, it is not yet possible to define a reliable mathematical model for the *Y* and *Z* site assignments of other trivalent cations (Fe, V, Cr), although important indications on their crystal-chemical behavior have been mentioned above.

Possible improvements of the nomenclature of oxy-tourmalines

Based on the strong correlation between ^{Z}Al and $^{[6]}$Al, and on the preference of R^{2+}- and R^{3+}-cations for the *Y* and *Z* sites, the recommended procedure of Henry et al. (2013) for allocating cations to *Z* and *Y* can be reformulated as follows.

(i) Initially assign Al^{3+} (in excess of that assigned to the *T* site) to the *Z* site according to equation (4), and then assign the remaining Al^{3+} to the *Y* site.

(ii) Next, successively assign Mg^{2+} to *Z* (up to 2 apfu), Cr^{3+}, V^{3+} and Fe^{3+}.

(iii) If there is an excess of trivalent cations at the *Z* site, the excess trivalent cations go into the *Y* site.

In this way, the resulting cation distributions should more closely conform to the actual *Y*- and *Z*-site occupancy with respect to the previous procedure. Therefore, for the given bulk composition, the combination of the new procedure for the *Y* and *Z* cation distributions with the recommendations of Henry et al. (2011) for the allocation of constituents over the *X*, *T*, *B*, O1 and O3 sites would yield a calculated structural formula leading to an end-member formula of a recognized tourmaline species. With regard to samples of Table 5, they can be univocally identified by applying the present procedure. In particular, sample drv18 may be identified as bosiite, ruling out the occurrence of a new species.

IMPLICATIONS

The definition of the crystal-chemical behavior of important constituents of tourmaline has allowed developing of a better scheme for site assignment that reveal major agreement and significant improvements compared to the earlier proposed scheme. The development of an unambiguous classification scheme is not just a question about terminology, but is a necessary step to understand the processes that govern the mineral diversity and has direct implications on the petrogenetic and provenence information of minerals. For example, ambiguity in the naming of a tourmaline species will not assist direct comparisons of tourmalines originating from different deposits. Therefore, for classification purposes, it would be better to treat all tourmalines alike, that is, follow recommendations based on assumptions whether or not a set of structural and spectroscopic data are available to determine real site occupancies. In this way, the naming of a tourmaline composition would be comparable for fully characterized tourmalines and for tourmalines for which only a chemical analysis is available. It would be appropriate to use the empirical structural formula to define new species, and the calculated structural formula to classify known species.

ACKNOWLEDGEMENTS

Funding by Sapienza University of Rome (Prog. Università 2016 to F.B.) is gratefully acknowledged. This study was presented at the Tourmaline 2017 symposium, Nové Město na Moravě, Czech Republic, June 23-28, 2017. I thank H. Skogby and the reviewers F.C. Hawthorne and A. Ertl for their useful suggestions that improved this work.

REFERENCES CITED

Akizuki, M., Kuribayashi, T., Nagase, T., and Kitakaze, A. (2001) Triclinic liddicoatite and elbaite in growth sectors of tourmaline from Madagascar. American Mineralogist, 86, 364–369.

Bačík, P., Cempírek, J., Uher, P., Novák, M., Ozdín, D., Filip, J., Škoda, R., Breiter, K., Klementová, M., and Ďuďa, R. (2013) Oxy-schorl, $Na(Fe_2^{2+}Al)Al_6Si_6O_{18}(BO_3)_3(OH)_3O$, a new mineral from Zlatá Idka, Slovak Republic and Příb slavice, Czech Republic. American Mineralogist, 98, 485–492.

Bačík, P., Ertl, A., Števko, M., Giester, G., and Sečkár, P. (2015) Acicular zoned tourmaline (magnesio-foitite to foitite) from a quartz vein near Tisovec, Slovakia: the relationship between crystal chemistry and acicular habit. Canadian Mineralogist, 53, 221–234.

Berryman, E.J., Wunder, B., Ertl, A., Koch-Müller, M., Rhede, D., Scheidl, K., Giester, G., and Heinrich, W. (2016) Influence of the X-site composition on tourmaline's crystal structure: Investigation of synthetic K-dravite, dravite, oxy-uvite, and magnesio-foitite using SREF and Raman spectroscopy. Physics and Chemistry of Minerals, 43, 83–102.

Bosi, F. (2008) Disordering of Fe^{2+} over octahedrally coordinated sites of tourmaline. American Mineralogist, 93, 1647–1653.

Bosi, F. (2010) Octahedrally coordinated vacancies in tourmaline: a theoretical approach. Mineralogical Magazine, 74, 1037–1044.

Bosi, F. (2011) Stereochemical constraints in tourmaline: from a short-range to a long-range structure. Canadian Mineralogist, 49, 17–27.

Bosi, F. (2013) Bond-valence constraints around the O1 site of tourmaline. Mineralogical Magazine, 77, 343–351.

Bosi, F. (2014) Mean bond length variation in crystal structures: a bond valence approach. Acta Crystallographica, B70, 697–704.

Bosi, F., and Andreozzi, G.B. (2013) A critical comment on Ertl et al. (2012): "Limitations of Fe^{2+} and Mn^{2+} site occupancy in tourmaline: Evidence from Fe^{2+}- and Mn^{2+}-rich tourmaline. American Mineralogist, 98, 2183–2192.

Bosi, F., and Lucchesi, S. (2007) Crystal chemical relationships in the tourmaline group: structural constraints on chemical variability. American Mineralogist, 92, 1054–1063.

Bosi, F., and Skogby, H. (2013) Oxy-dravite, $Na(Al_2Mg)(Al_5Mg)(Si_6O_{18})(BO_3)_3(OH)_3O$, a new mineral species of the tourmaline supergroup. American Mineralogist, 98, 1442–1448.

Bosi, F., Balić-Žunić, T., and Surour, A.A. (2010) Crystal structure analysis of four tourmalines from the Cleopatra's Mines (Egypt) and Jabal Zalm (Saudi Arabia), and the role of Al in the tourmaline group. American Mineralogist, 95, 510–518.

Bosi, F., Reznitskii, L., and Skogby, H. (2012) Oxy-chromium-dravite, $NaCr_3(Cr_4Mg_2)(Si_6O_{18})(BO_3)_3(OH)_3O$, a new mineral species of the tourmaline supergroup. American Mineralogist, 97, 2024–2030.

Bosi, F., Andreozzi, G.B., Skogby, H., Lussier, A.J., Abdu, Y., and Hawthorne, F.C. (2013a) Fluor-elbaite, $Na(Li_{1.5}Al_{1.5})Al_6(Si_6O_{18})(BO_3)_3(OH)_3F$, a new mineral species of the tourmaline supergroup. American Mineralogist, 98, 297–303.

Bosi, F., Reznitskii, L., and Sklyarov, E.V. (2013b) Oxy-vanadium-dravite, $NaV_3(V_4Mg_2)(Si_6O_{18})(BO_3)_3(OH)_3O$: crystal structure and redefinition of the "vanadium-dravite" tourmaline. American Mineralogist, 98, 501–505.

Bosi, F., Skogby, H., Hålenius, U., and Reznitskii, L. (2013c) Crystallographic and spectroscopic characterization of Fe-bearing chromo-alumino-povondraite and its relations with oxy-chromium-dravite and oxy-dravite. American Mineralogist, 98, 1557–1564.

Bosi, F., Reznitskii, L., Skogby, H., and Hålenius, U. (2014a) Vanadio-oxy-chromium-dravite, $NaV_3(Cr_4Mg_2)(Si_6O_{18})(BO_3)_3(OH)_3O$, a new mineral species of the tourmaline supergroup. American Mineralogist, 99, 1155–1162.

Bosi, F., Skogby, H., Reznitskii, L., and Hålenius, U. (2014b) Vanadio-oxy-dravite, $NaV_3(Al_4Mg_2)(Si_6O_{18})(BO_3)_3(OH)_3O$, a new mineral species of the tourmaline supergroup. American Mineralogist, 99, 218–224.

446 Bosi, F., Andreozzi, G.B., Hålenius, U. and Skogby, H. (2015a) Experimental evidence for partial
447 Fe^{2+} disorder at the *Y* and *Z* sites of tourmaline: a combined EMP, SREF, MS, IR and OAS
448 study of schorl. Mineralogical Magazine, 79, 515–528.
449 Bosi, F., Andreozzi, G.B., Agrosì, G., and Scandale, E. (2015b) Fluor-tsilaisite,
450 $NaMn_3Al_6(Si_6O_{18})(BO_3)_3(OH)_3F$, a new tourmaline from San Piero in Campo (Elba, Italy)
451 and new data on tsilaisitic tourmaline from the holotype specimen locality. Mineralogical
452 Magazine, 79, 89–101.
453 Bosi, F., Skogby, H., Lazor, P., Reznitskii, L. (2015c) Atomic arrangements around the O3 site in
454 Al- and Cr-rich oxy-tourmalines: a combined EMP, SREF, FTIR and Raman study. Physics
455 and Chemistry of Minerals, 42, 441–453.
456 Bosi, F., Skogby, H., and Hålenius, U. (2016a) Thermally induced cation redistribution in Fe-
457 bearing oxy-dravite and potential geothermometric implications. Contribution to Mineralogy
458 and Petrology, 171, 47.
459 Bosi F, Skogby H, Balić-Žunić T (2016b) Thermal stability of extended clusters in dravite: a
460 combined EMP, SREF and FTIR study. Physics and Chemistry of Minerals, 43, 395–407.
461 Bosi, F., Skogby H., Ciriotti M.E., Gadas P., Novák M., Cempírek J., Všianský D., and Filip J.
462 (2017a) Lucchesiite, $CaFe^{2+}{}_3Al_6(Si_6O_{18})(BO_3)_3(OH)_3O$, a new mineral species of the
463 tourmaline supergroup. Mineralogical Magazine, 81, 1–14.
464 Bosi, F., Reznitskii, L., Hålenius, U. and Skogby, H. (2017b) Crystal chemistry of Al-V-Cr oxy-
465 tourmalines from Sludyanka complex, Lake Baikal, Russia. European Journal of
466 Mineralogy, 29, 457–472.
467 Bosi, F., Cámara, F., Ciriotti, M.E., Hålenius, U., Reznitskii, L., and Stagno, V. (2017c) Crystal-
468 chemical relations and classification problems of tourmalines belonging to the oxy-schorl–
469 oxy-dravite–bosiite–povondraite series. European Journal of Mineralogy, 29, 445–455.

Bosi, F., Skogby, H., and Hålenius, U. (2017d) Oxy-foitite, □$(Fe^{2+}Al_2)Al_6(Si_6O_{18})(BO_3)_3(OH)_3O$, a new mineral species of the tourmaline supergroup. European Journal of Mineralogy, DOI 10.1127/ejm/2017/0029-2631.

Brown, I.D. (2016) The chemical bond in inorganic chemistry: the bond valence model, 2nd ed. Oxford University Press, U.K..

Cempírek, J., Houzar, S., Novák, M., Groat, L.A., Selway, J.B., and Šrein, V. (2013) Crystal structure and compositional evolution of vanadium-rich oxy-dravite from graphite quartzite at Bítovánky, Czech Republic. Journal of Geosciencies, 58, 149–162.

Clark, C.M., Hawthorne, F.C., and Ottolini, L. (2011) Fluor-dravite, $NaMg_3Al_6Si_6O_{18}(BO_3)_3(OH)_3F$, a new mineral species of the tourmaline group from the Crabtree emerald mine, Mitchell County, North Carolina: description and crystal structure. Canadian Mineralogist, 49, 57–62.

Dutrow, B.L., and Henry, D.J. (2011) Tourmaline: A geologic DVD. Elements, 7, 301–306.

Ertl, A., Hughes, J.M., Pertlik, F., Foit, F.F. Jr, Wright, S.E., Brandstatter, F., and Marler, B. (2002) Polyhedron distortions in tourmaline. Canadian Mineralogist, 40,153–162.

Ertl, A., Kolitsch, U., Prowatke, S., Dyar, M.D., and Henry, D.J. (2006) The F-analog of schorl from Grasstein, Trentino–South Tyrol, Italy: crystal structure and chemistry. European Journal of Mineralogy, 18, 583–588.

Ertl, A., Hughes, J.M., Prowatke, S., Ludwig, T., Brandstätter, F., Körner, W., and Dyar, M.D. (2007) Tetrahedrally-coordinated boron in Li-bearing olenite from "mushroom" tourmaline from Momeik, Myanmar: structure and chemistry. Canadian Mineralogist, 45, 891–899.

Ertl, A., Tillmanns, E., Ntaflos, T., Francis, C., Giester, G., Korner, W., Hughes, J.M., Lengauer, C., and Prem, M. (2008a) Tetrahedrally coordinated boron in Al-rich tourmaline and its relationship to the pressure-temperature conditions of formation. European Journal of Mineralogy, 20, 881–888.

Ertl, A., Rossman, G.R., Hughes, J.M., Ma, C., and Brandstätter, F. (2008b) V^{3+}-bearing, Mg-rich, strongly disordered olenite from a graphite deposit near Amstall, Lower Austria: A structural, chemical and spectroscopic investigation. Neues Jahrbuch für Mineralogie Abhandlungen, 184, 243–253.

Ertl, A., Kolitsch, U., Meyer, H.-P., Ludwig, T., Lengauer, C.L., Nasdala, L., and Tillmanns, E. (2009) Substitution mechanism in tourmalines of the "fluor-elbaite"-rossmanite series from Wolkenburg, Saxony, Germany. Neues Jahrbuch für Mineralogie Abhandlungen, 186, 51–61.

Ertl, A., Rossman, G.R., Hughes, J.M., London, D., Wang, Y., O'Leary, J.A., Dyar, M.D., Prowatke, S., Ludwig, T., and Tillmanns, E. (2010a) Tourmaline of the elbaite-schorl series from the Himalaya Mine, Mesa Grande, California, U.S.A.: A detailed investigation. American Mineralogist, 95, 24–40.

Ertl, A., Marschall, H.R., Giester, G., Henry, D.J., Schertl, H.-P., Ntaflos, T., Luvizotto, G.L., Nasdala, L., and Tillmanns, E. (2010b) Metamorphic ultra high-pressure tourmalines: Structure, chemistry, and correlations to PT conditions. American Mineralogist, 95, 1–10.

Ertl, A., Mali, H., Schuster, R., Körner, W., Hughes, J.M., Brandstätter, F., and Tillmanns, E. (2010c) Li-bearing, disordered Mg-rich tourmalines from the pegmatite-marble contact from the Austroalpine basement units (Styria, Austria). Mineralogy and Petrology, 99, 89–104.

Ertl, A., Schuster, R., Hughes, J.M., Ludwig, T., Meyer, H.-P., Finger, F., Dyar, M.D., Ruschel, K., Rossman, G.R., Klötzi, U., Brandstätter, F., Lengauer, C.L., and Tillmans, E. (2012a) Li-bearing tourmalines in Variscan granitic pegmatites from the Moldanubian nappes, Lower Austria. European Journal of Mineralogy, 24, 695–715.

Ertl, A., Giester, G., Ludwig, T., Meyer, H.-P., and Rossman, G.R. (2012b) Synthetic B-rich olenite: Correlations of single-crystal structural data. American Mineraleralogist, 97, 1591–1597.

Ertl, A., Kolitsch, U., Dyar, M.D., Hughes, J.M., Rossman, G.R., Pieczka, A., Henry, D.J., Pezzotta, F., Prowatke, S., Lengauer, C.L., Körner, W., Brandstätter, F., Francis, C.A., Prem, M., and Tillmanns, E. (2012c). Limitations of Fe^{2+} and Mn^{2+} site occupancy in tourmaline: evidence from Fe^{2+}- and Mn^{2+}-rich tourmaline. American Mineralogist, 97, 1402–1416.

Ertl, A., Giester, G., Schüssler, U., Brätz, H., Okrusch, M., Tillmanns, E., and Bank, H. (2013) Cu- and Mn-bearing tourmalines from Brazil and Mozambique: Crystal structures, chemistry and Correlations. Mineralogy and Perology, 107, 265–279.

Ertl, A., Vereshchagin, O.S., Giester, G., Tillmanns, E., Meyer, H.-P., Ludwig, T., Rozhdestvenskaya, I.V., and Frank-Kamenetskaya, O.V. (2015) Structural and chemical investigation of a zoned synthetic Cu-rich tourmaline. Canadian Mineralogist, 53, 209–220.

Ertl, A., Baksheev, I.A., Giester, G., Lengauer, C.L., Prokofiev, V.Y., and Zorina, L.D. (2016a) Bosiite, $NaFe^{3+}_3(Al_4Mg_2)(Si_6O_{18})(BO_3)_3(OH)_3O$, a new ferric member of the tourmaline supergroup from the Darasun gold deposit, Transbaikalia, Russia. European Journal of Mineralogy, 28, 581–591.

Ertl, A., Kolitsch, U., Dyar, M.D., Meyer, H.-P., Henry, D.J., Rossman, G.R., Prem, M., Ludwig, T., Nasdala, L., Lengauer, C.L., Tillmanns E., and Niedermayr, G. (2016b) Fluor-schorl, a new member of the tourmaline supergroup, and new data on schorl from the cotype localities. European Journal of Mineralogy, 28, 163–177.

Filip, J., Bosi, F., Novák, M., Skogby, H., Tuček, J., Čuda, J., and Wildner, M. (2012) Redox processes of iron in the tourmaline structure: Example of the high-temperature treatment of Fe3+-rich schorl. Geochimica et Cosmochimica Acta, 86, 239–256.

Gatta, G.D., Danisi, R.M., Adamo, I., Meven, M., and Diella, V. (2012) A single-crystal neutron and X-ray diffraction study of elbaite. Physics and Chemistry of Minerals, 39, 577–588.

544 Gibbs, G.V., Ross, N.L., Cox, D.F., and Rosso, K.M. (2014) Insights into the crystal chemistry of
545 Earth materials rendered by electron density distributions: Pauling's rules revisited.
546 American Mineralogist, 99, 1071–1084.
547 Grew, E.S., Krivovichev, S.V., Hazen, R.M., and Hystad, G. (2016) Evolution of structural
548 complexity in boron minerals. Canadian Mineralogist, 54,125–143.
549 Grew, E.S., Bosi, F., Gunter, M., Hålenius, U., Trumbull, R.B., and Yates, M.G. (2017) Fluor-
550 elbaite, lepidolite and Ta-Nb oxides from a pegmatite of the 3000 MA Sinceni pluton,
551 Swaziland: Evidence for lithium-cesium-tantalum (LCT) pegmatites in the Mesoarchean.
552 European Journal of Mineralogy, DOI 10.1127/ejm/2017/0029-2686
553 Hatert, F., and Burke, E.A.J. (2008) The IMA–CNMNC dominant-constituent rule revisited and
554 extended. Canadian Mineralogist, 46, 717–728.
555 Hawthorne, F.C. (1996) Structural mechanisms for light-element variations in tourmaline. Canadian
556 Mineralogist, 34, 123–132.
557 Hawthorne, F.C. (2002) Bond-valence constraints on the chemical composition of tourmaline.
558 Canadian Mineralogist, 40, 789–797.
559 Hawthorne, F.C. (editor) (2006) Landmark Papers: Structure Topology. The Mineralogical Society
560 of Great Britain and Ireland, London.
561 Hawthorne, F.C. (2016) Short-range atomic arrangements in minerals. I: the minerals of the
562 amphibole, tourmaline and pyroxene supergroups. European Journal of Mineralogy, 28,
563 513–536.
564 Hawthorne, F.C., and Dirlam, D.M. (2011) Tourmaline the indicator mineral: from atomic
565 arrangement to Viking navigation. Elements, 7, 307–312.
566 Hawthorne, F.C., and Henry, D. (1999) Classification of the minerals of the tourmaline group.
567 European Journal of Mineralogy, 11, 201–215.

568 Hawthorne, F.C.H., Della Ventura, G., Oberti , R., Robert, J.-L., and Iezzi, G. (2005) Short-range
569 order in minerals: amphiboles. Canadian Mineralogist, 43, 1895–1920.
570 Henry, D.J., and Dutrow, B.L. (2011) The incorporation of fluorine in tourmaline: Internal
571 crystallographic controls or external environmental influences? Canadian Mineralogist, 49,
572 41–56.
573 Henry, D.J., Novák, M., Hawthorne, F.C., Ertl, A., Dutrow, B.L., Uher, P., and Pezzotta, F. (2011)
574 Nomenclature of the tourmaline-supergroup minerals. American Mineralogist, 96, 895–913.
575 Henry, D.J., Novák, M., Hawthorne, F.C., Ertl, A., Dutrow, B.L., Uher, P., and Pezzotta, F. (2013)
576 Erratum. American Mineralogist, 98, 524.
577 Hughes, J.M., Rakovan, J., Ertl, A., Rossman, G.R., Baksheev, I., and Bernhardt, H.-J. (2011)
578 Dissymmetrization in tourmaline: the atomic arrangement of sectorally zoned triclinic Ni-
579 bearing dravite. Canadian Mineralogist, 49, 29–40.
580 Kihara, K., Hirata, H., Ida, A., Okudera, H., and Morishita, T. (2007) An X-ray single crystal study
581 of asymmetric thermal vibrations and the positional disorder of atoms in elbaite. Journal of
582 Mineralogical and Petrological Sciences, 102, 115–126.
583 Krivovichev, S.V. (2013) Structural complexity of minerals: Information storage and processing in
584 the mineral world. Mineralogical Magazine, 77, 275–326.
585 Kutzschbach, M., Wunder, B., Rhede, D., Koch-Müller, M., Ertl, A., Giester, G., Heinrich, W., and
586 Franz, G. (2016) Tetrahedral boron in natural and synthetic high-pressure tourmaline:
587 Evidence from Raman spectroscopy. American Mineralogist, 101, 93–104.
588 Kutzschbach, M., Wunder, B., Krstulovic, M., Ertl, A., Trumbull, R., Rocholl, A., and Giester, G.
589 (2017) First high-pressure synthesis of rossmanitic tourmaline and evidence for the
590 incorporation of Li at the X site. Physics and Chemistry of Minerals, 44, 353–363.
591 London, D. (2011) Experimental synthesis and stability of tourmaline: a historical perspective.
592 Canadian Mineralogist, 49, 117–136.

London, D., Ertl, A., Hughes, J.M., Morgan VI, G.B., Fritz, E.A., and Harms, B.S. (2006) Synthetic Ag-rich tourmaline: Structure and chemistry. American Mineralogist, 91, 680–684.

Lussier, A.J., Aguiar, P.M., Michaelis, V.K., Kroeker, S., Herwig, S., Abdu, Y., and Hawthorne, F.C. (2008) Mushroom elbaite from the Kat Chay mine, Momeik, near Mogok, Myanmar: I. Crystal chemistry by SREF, EMPA, MAS NMR and Mössbauer spectroscopy. Mineralogical Magazine, 72, 747–761.

Lussier, A.J., Hawthorne, F.C., Abdu, Y., Herwig, S., Michaelis, V.K., Aguiar, P.M., and Kroeker, S. (2011a) The crystal chemistry of "wheatsheaf" tourmaline from Mogok, Myanmar. Mineralogical Magazine, 72, 999–1010.

Lussier, A.J., Abdu, Y. Hawthorne, F.C., Michaelis, V.K., Aguiar, P.M., and Kroeker, S. (2011b) Oscillatory zoned liddicoatite from Anjanabonoina, central Madagascar. I. Crystal chemistry and structure by SREF and ^{11}B and ^{27}Al MAS NMR spectroscopy. Canadian Mineralogist, 49, 63–88.

Lussier, A., Ball, N.A., Hawthorne, F.C., Henry, D.J., Shimizu, R., Ogasawara, Y., and Ota, T. (2016) Maruyamaite, $K(MgAl_2)(Al_5Mg)Si_6O_{18}(BO_3)_3(OH)_3O$, a potassium-dominant tourmaline from the ultrahigh-pressure Kokchetav massif, northern Kazakhstan: description and crystal structure. American Mineralogist, 101, 355–361.

Marler, B., Borowski, M., Wodara, U., and Schreyer, W. (2002) Synthetic tourmaline (olenite) with excess boron replacing silicon in the tetrahedral site: II. Structure analysis. European Journal of Mineralogy, 14, 763–771.

Marschall, H.R., Korsakov, A.V., Luvizotto, G.L., Nasdala, L., and Ludwig, T. (2009) On the occurrence and boron isotopic composition of tourmaline in (ultra)high-pressure metamorphic rocks. Journal of the Geological Society, 166, 811–823.

Nickel, E.H., and Grice, J.D. (1998) The IMA Commission on New Minerals and Mineral Names: procedures and guidelines on mineral nomenclature. Canadian Mineralogist, 36, 913–926.

Nishio-Hamane, D.,Minakawa, T., Yamaura, J., Oyama, T., Ohnishi, M., and Shimobayashi, N. (2014) Adachiite, a Si–poor member of the tourmaline supergroup from the Kiura mine, Oita Prefecture, Japan. Journal of Mineralogical and Petrological Sciences, 109, 74–78.

Novák, M., Ertl, A., Povondra, P., Galiová, M.V., Rossman, G.R., Pristacz, H., Prem, M., Giester, G., Gadas, P., and Škoda, R. (2013a) Darrellhenryite, $Na(LiAl_2)Al_6(BO_3)_3Si_6O_{18}(OH)_3O$, a new mineral from the tourmaline supergroup. American Mineralogist, 98, 1886–1892.

Razmanova, Z.P., Kornetova, V.A., Shipko, M.N., and Belov, N.B. (1983) Refinements in crystal structure and configuration of iron-bearing uvite. Trudy AN SSSR, Mineralogicheskiy Muzey im. A.E. Fersmana, 31, 108-116 (in Russian).

Reznitskii, L., Clark, C.M., Hawthorne, F.C., Grice, J.D., Skogby, H., Hålenius, U., and Bosi, F. (2014) Chromo-alumino-povondraite, $NaCr_3(Al_4Mg_2)(Si_6O_{18})(BO_3)_3(OH)_3O$, a new mineral species of the tourmaline supergroup. American Mineralogist, 99, 1767–1773.

Rozhdestvenskaya, I.V., Bronzova, Yu.M., Frank-Kamenetskaya, O.V., Zolotarev, A.A., Kuznetsova, L.G., and Bannova, I.I. (2008) Refinement of the Crystal Structure of Calcium–Lithium–Aluminum Tourmaline from the Pegmatite Vein in the Sangilen Upland (Tuva Republic). Crystallography Reports, 53, 223–227.

Rozhdestvenskayaa, I.V., Setkovab, T.V., Vereshchagina, O.S., Shtukenberga, A.G., and Shapovalovb, Yu.B. (2012) Refinement of the crystal structures of synthetic nickel- and cobalt-bearing tourmalines. Crystallography Reports, 57, 57–63.

Shannon, R.D. (1976) Revised effective ionic radii and systematic studies of interatomic distances in halides and chalcogenides. Acta Crystallographica, A32, 751-767.

Shtukenberg, A., Rozhdestvenskaya, I., Frank-Kamenetskaya, O., Bronzova, J., Euler, H., Kirfel, A., Bannova, I., and Zolotarev, A. (2007) Symmetry and crystal structure of biaxial elbaite-liddicoatite tourmaline from the Transbaikalia region, Russia. American Mineralogist, 92, 675–686.

643 Skogby, H., Bosi, F., and Lazor, P. (2012) Short-range order in tourmaline: a vibrational
644 spectroscopic approach to elbaite. Physics and Chemistry of Minerals, 39, 811–816.
645 van Hinsberg, V.J., Henry, D.J., and Marschall, H.R. (2011) Tourmaline: an ideal indicator of its
646 host environment. Canadian Mineralogist, 49, 1–16.
647 Vereshchagin, O.S., Rozhdestvenskaya, I.V., Frank- Kamenetskaya, O.V., Zolotarev, A.A., and
648 Mashkovtsev, R.I. (2013) Crystal chemistry of Cu-bearing tourmalines. American
649 Mineralogist, 98, 1610–1616.
650 Vereshchagin, O.S., Rozhdestvenskaya, I.V., Frank-Kamenetskaya, O.V., and Zolotarev, A.A.
651 (2014) Ion substitutions and structural adjustment in Cr-bearing tourmalines. European
652 Journal of Mineralogy, 26, 309–321.
653 Vereshchagin, O.S., Frank-Kamenetskaya, O.V., and Rozhdestvenskaya, I.V. (2015) Crystal
654 structure and stability of Ni-rich synthetic tourmaline. Distribution of divalent transition-
655 metal cations over octahedral positions, Mineralogical Magazine, 79, 997–1006.
656 Vereshchagin, O.S., Setkova, T.V., Rozhdestvenskaya, I.V., Frank-Kamenetskaya, O.V., Deyneko,
657 D.V., and Pokholok, K.V. (2016) Synthesis and crystal structure of Ga-rich, Fe-bearing
658 tourmaline, European Journal of Mineralogy, 28, 593–599.
659 Watenphul, A., Burgdorf, M., Schlüter, J., Horn, I., Malcherek, T., and Mihailova, B. (2016)
660 Exploring the potential of Raman spectroscopy for crystallochemical analyses of complex
661 hydrous silicates: II. Tourmalines. American Mineralogist, 101, 970–985.
662
663

List of tables

List of figures and figure captions

(2011), **3** Filip et al. (2012), **1** Gatta et al. (2012), **2** Cempírek et al. (2013), **3** Bačík et al. (2013, 2015), **1** Novák et al. (2013), **9** Vereshchagin et al. (2013, 2014, 2015, 2016), **1** Reznitskii et al. (2014), **1** Nishio-Hamane et al. (2014), **2** Kutzschbach et al. (2016, 2017), **3** Berryman et al. (2016), **1** Watenphul et al. (2016), **1** Grew et al. (2017), **7** Bosi et al. (submitted), **10** Bosi (unpublished).

FIGURE 4. Plot of maximum occupancy of $^{Z}R^{2+}$ observed in tourmalines with Al > 5 apfu against R^{2+}-Al^{3+} cation-size mismatch. Solid line is linear regression. Data from Rozhdestvenskaya et al. (2012), Filip et al. (2012), Bosi and Skogby (2013) and Bosi et al. (2015b).

FIGURE 5. Variation in ^{Z}Al as a function of $^{[6]}Al$ in oxy-tourmalines ($^{O1}O^{2-}$ > 0.5 apfu). Solid line is quadratic regression. Dashed diagonal line is ratio 1:1 between ^{Z}Al and $^{[6]}Al$. Plot obtained using 83 data sets accompanied by SREF: 34 from Bosi and Lucchesi (2007, references therein) plus a total of 48 from **1** Bosi (2008), **5** Ertl et al. (2008b, 2010b, 2012b, 2015, 2016a), **26** Bosi et al. (2010, 2012, 2013b, 2013c, 2014a, 2014b, 2015c, 2017b, 2017c), **1** Rozhdestvenskaya et al. (2012), **1** Bosi and Skogby (2013), **2** Cempírek et al. (2013), **2** Bačík et al. (2013), **1** Novák et al. (2013), **5** Vereshchagin et al. (2013, 2014, 2016), **1** Reznitskii et al. (2014), **1** Watenphul et al. (2016), **1** Lussier et al. (2016), **1** Kutzschbach et al. (2017), **1** Bosi et al. (submitted).

This is a preprint, the final version is subject to change, of the American Mineralogist (MSA)
Cite as Authors (Year) Title. American Mineralogist, in press.
(DOI will not work until issue is live.) DOI: http://dx.doi.org/10.2138/am-2017-6289

Table 1. The 26 relevant constituents occurring in tourmaline

Valence	zero	1	2	3	4
	$^{[9]}$-$^{[6]}$□	**$^{[9]}Na^{+}$** **$^{[9]}K^{+}$** **$^{[6]}Li^{+}$** $^{[9]}Ag^{+}$ **H^{+}** **$^{[3]}F^{-}$**	**$^{[9]}Ca^{2+}$** **$^{[6]}Mg^{2+}$** **$^{[6]}Fe^{2+}$** **$^{[6]}Mn^{2+}$** $^{[6]}Ni^{2+}$ $^{[6]}Co^{2+}$ $^{[6]}Cu^{2+}$ $^{[6]}Zn^{2+}$ **$^{[3]}$-$^{[4]}O^{2-}$**	**$^{[6]}$-$^{[4]}Al^{3+}$** **$^{[6]}Cr^{3+}$** **$^{[6]}V^{3+}$** **$^{[6]}Fe^{3+}$** $^{[6]}Ga^{3+}$ **$^{[3]}$-$^{[4]}B^{3+}$** $^{[6]}Mn^{3+}$	**$^{[4]}Si^{4+}$** $^{[6]}Ti^{4+}$

Notes: Vacancy (=□) is considered as a constituent in accord with the IMA-CNMNC rules. In brackets are indicated coordination numbers. In bold are indicated constituents characterizing the 33 species of the tourmaline-supergroup minerals.

Table 2. The 33 mineral species of tourmaline recognized by the IMA-CNMNC

Adachiite	$CaFe^{2+}_3Al_6(Si_5AlO_{18})(BO_3)_3(OH)_3OH$
Bosiite	$NaFe^{3+}_3(Al_4Mg_2)Si_6O_{18}(BO_3)_3(OH)_3O$
Chromium-dravite	$NaMg_3Cr_6Si_6O_{18}(BO_3)_3(OH)_3OH$
Chromo-alumino-povondraite	$NaCr_3(Al_4Mg_2)Si_6O_{18}(BO_3)_3(OH)_3O$
Darrellhenryite	$NaLiAl_2Al_6Si_6O_{18}(BO_3)_3(OH)_3O$
Dravite	$NaMg_3Al_6Si_6O_{18}(BO_3)_3(OH)_3OH$
Elbaite	$Na(Li_{1.5},Al_{1.5})Al_6Si_6O_{18}(BO_3)_3(OH)_3OH$
Feruvite	$CaFe^{2+}_3(MgAl_5)Si_6O_{18}(BO_3)_3(OH)_3OH$
Fluor-buergerite	$NaFe^{3+}_3Al_6Si_6O_{18}(BO_3)_3O_3F$
Fluor-dravite	$NaMg_3Al_6Si_6O_{18}(BO_3)_3(OH)_3F$
Fluor-elbaite	$Na(Li_{1.5},Al_{1.5})Al_6Si_6O_{18}(BO_3)_3(OH)_3F$
Fluor-liddicoatite	$Ca(Li_2Al)Al_6Si_6O_{18}(BO_3)_3(OH)_3F$
Fluor-schorl	$NaFe^{2+}_3Al_6Si_6O_{18}(BO_3)_3(OH)_3F$
Fluor-tsilaisite	$NaMn^{2+}_3Al_6Si_6O_{18}(BO_3)_3(OH)_3F$
Fluor-uvite	$CaMg_3(Al_5Mg)Si_6O_{18}(BO_3)_3(OH)_3F$
Foitite	$\square(Fe^{2+}_2Al)Al_6Si_6O_{18}(BO_3)_3(OH)_3OH$
Lucchesiite	$CaFe^{2+}_3Al_6Si_6O_{18}(BO_3)_3(OH)_3O$
Luinaite-(OH) [a]	$(Na,\square)(Fe^{2+},Mg)_3Al_6Si_6O_{18}(BO_3)_3(OH)_3OH$
Magnesio-foitite	$\square(Mg_2Al)Al_6Si_6O_{18}(BO_3)_3(OH)_3OH$
Maruyamaite	$K(Al_2Mg)(Al_5Mg)Si_6O_{18}(BO_3)_3(OH)_3O$
Olenite	$NaAl_3Al_6Si_6O_{18}(BO_3)_3O_3OH$
Oxy-chromium-dravite	$NaCr_3(Cr_4Mg_2)Si_6O_{18}(BO_3)_3(OH)_3O$
Oxy-dravite	$Na(Al_2Mg)(Al_5Mg)Si_6O_{18}(BO_3)_3(OH)_3O$
Oxy-foitite	$\square(Al_2Fe^{2+})Al_6Si_6O_{18}(BO_3)_3(OH)_3O$
Oxy-schorl	$Na(Fe^{2+}_2Al)Al_6Si_6O_{18}(BO_3)_3(OH)_3O$
Oxy-vanadium-dravite	$NaV_3(V_4Mg_2)Si_6O_{18}(BO_3)_3(OH)_3O$
Povondraite	$NaFe^{3+}_3(Fe^{3+}_4Mg_2)Si_6O_{18}(BO_3)_3(OH)_3O$
Rossmanite	$\square(Al_2Li)Al_6Si_6O_{18}(BO_3)_3(OH)_3OH$
Schorl	$NaFe^{2+}_3Al_6Si_6O_{18}(BO_3)_3(OH)_3OH$
Tsilaisite	$NaMn^{2+}_3Al_6Si_6O_{18}(BO_3)_3(OH)_3OH$
Uvite	$CaMg_3(Al_5Mg)Si_6O_{18}(BO_3)_3(OH)_3OH$
Vanadio-oxy-chromium-dravite	$NaV_3(Cr_4Mg_2)Si_6O_{18}(BO_3)_3(OH)_3O$
Vanadio-oxy-dravite	$NaV_3(Al_4Mg_2)Si_6O_{18}(BO_3)_3(OH)_3O$

[a] Mineral (IMA 2009-046) description has not yet been published in the scientific literature

This is a preprint, the final version is subject to change, of the American Mineralogist (MSA)
Cite as Authors (Year) Title. American Mineralogist, in press.
(DOI will not work until issue is live.) DOI: http://dx.doi.org/10.2138/am-2017-6289

TABLE 3. Stable local charge arrangements around the O1 and O3 sites of tourmaline derived from Hawthorne (1996, 2002) and Bosi (2010, 2011, 2013)

Composition	Formal valence	Charge arrangement	MFV [a]
O1	**O1** [b]	***YYY***	**<*Y*>**
(OH) or F	–1	(R^{3+} + $2R^{+}$)	+1.67
(OH) or F	–1	(R^{3+} + R^{2+} + □)	+1.67
(OH) or F	–1	(R^{3+} + R^{2+} + R^{+})	+2.00
(OH) or F	–1	(R^{3+} + R^{3+} + □)	+2.00
(OH) or F	–1	($3R^{2+}$)	+2.00
(OH) or F	–1	($2R^{3+}$ + R^{+})	+2.33
(OH) or F	–1	($2R^{2+}$ + R^{3+})	+2.33
O	–2	(R^{2+} + $2R^{3+}$)	+2.67
O	–2	($3R^{3+}$)	+3.00
O3	**O3** [b]	***YZZ***	**<*YZZ*>**
(OH)	–1	$^{Y}R^{+}$ + ^{Z}(R^{2+} + R^{3+})	+2.00
(OH)	–1	^{Y}□ + ^{Z}($2R^{3+}$)	+2.00
(OH)	–1	$^{Y}R^{+}$ + ^{Z}($2R^{3+}$)	+2.33
(OH)	–1	$^{Y}R^{2+}$ + ^{Z}(R^{2+} + R^{3+})	+2.33
(OH)	–1	$^{Y}R^{3+}$ + ^{Z}($2R^{2+}$)	+2.33
(OH)	–1	$^{Y}R^{2+}$ + ^{Z}($2R^{3+}$)	+2.67
(OH)	–1	$^{Y}R^{3+}$ + ^{Z}(R^{2+} + R^{3+})	+2.67
(OH)	–1	$^{Y}R^{3+}$ + ^{Z}($2R^{3+}$)	+3.00
O	–2	$^{Y}R^{3+}$ + ^{Z}($2R^{3+}$)	+3.00

Abbreviation: R^{+}, R^{2+} and R^{3+} = generalized monovalent (+1), divalent (+2) and trivalent (+3) cation

[a] MFV = mean formal valence = total charge/3

[b] Because of the hydrogen bond, the bond-valence sum at the O1 and O3 sites occupied by (OH) are 1.05 vu and 1.15 vu, respectively (e.g., Hawthorne 2002; Gatta et al. 2014)

TABLE 4. Empirical mean ionic radii (Å) for [6]-coordinated ions in tourmaline

Ion	This work	Shannon (1976)
Al^{3+}	0.547(3)	0.535
Cr^{3+}	0.615(1)	0.615
V^{3+}	0.655(1)	0.64
Fe^{3+}	0.675(15)	0.645
Fe^{2+}	0.776(1)	0.78
Mg^{2+}	0.722(1)	0.72
Mn^{2+}	0.809(1)	0.83
Li^{+}	0.751(9)	0.76

Notes: Empirical ionic radii from Shannon (1976) apply to the other ions such as Ti^{4+} = 0.605 , Ni^{2+} = 0.69 Å, Co^{2+} = 0.745 Å, etc.

The mean anionic radii <O> related to the *Y* and *Z* sites is function of constituent-anion radius of Shannon (1976). The $<^{Y}O>$ varies from 1.353 to 1.363 Å; $<^{Z}O>$ varies from 1.357 Å for tourmalines with O3 = (OH) to 1.360 Å for tourmalines with O3 = O^{2-}.

Estimated standard error (±σ) in brackets

TABLE 5. Examples of identification of selected oxy-tourmalines

Sample	PR1973	TM84a	PR85m	drv18
	Empirical site population			
Y	$V_{2.21}Cr_{0.54}Mg_{0.11}Fe^{3+}_{0.12}Ti_{0.01}Zn_{0.01}$	$Al_{1.52}Fe^{3+}_{0.06}Fe^{2+}_{1.07}Mg_{0.25}Mn^{2+}_{0.05}Zn_{0.01}Ti^{4+}_{0.03}$	$Al_{1.23}Fe^{2+}_{0.90}Mg_{0.63}Fe^{3+}_{0.15}Ti^{4+}_{0.09}$	$Mg_{1.35}Fe^{2+}_{0.94}Fe^{3+}_{0.49}Ti^{4+}_{0.20}$
Z	$Cr_{3.01}Al_{0.96}Mg_{2.03}$	$Al_{5.48}Fe^{3+}_{0.08}Mg_{0.36}Fe^{2+}_{0.08}$	$Al_{5.05}Mg_{0.89}Fe^{3+}_{0.06}$	$Al_{4.58}Mg_{0.80}Fe^{3+}_{0.62}$
Name	vanadio-oxy-chromium-dravite	oxy-foitite	oxy-schorl	*oxy-?*
	Calculated site population according to Henry *et al.* (2013)			
Y	$Cr_{2.72}Mg_{0.14}\ Fe^{3+}_{0.12}Ti_{0.01}Zn_{0.01}$	$Al_{1.00}Fe^{3+}_{0.14}Fe^{2+}_{1.15}Mg_{0.61}Mn^{2+}_{0.05}Zn_{0.01}Ti^{4+}_{0.03}$	$Mg_{1.52}Fe^{2+}_{0.90}Al_{0.28}Fe^{3+}_{0.21}Ti^{4+}_{0.09}$	$Mg_{0.73}Fe^{2+}_{0.94}Fe^{3+}_{1.11}Ti^{4+}_{0.20}$
Z	$Al_{0.96}Mg_{2.00}V_{2.21}Cr_{0.83}$	$Al_{6.00}$	$Al_{6.00}$	$Al_{4.58}Mg_{1.42}$
Name	*oxy-?*	*oxy-?*	oxy-dravite	*oxy-?*
	Calculated site population according to this work			
Y	$V_{2.21}Cr_{0.51}Mg_{0.14}Fe^{3+}_{0.12}Ti_{0.01}Zn_{0.01}$	$Al_{1.47}Fe^{3+}_{0.14}Fe^{2+}_{1.15}Mg_{0.14}Mn^{2+}_{0.05}Zn_{0.01}Ti^{4+}_{0.03}$	$Al_{1.10}Fe^{2+}_{0.90}Mg_{0.70}Fe^{3+}_{0.21}Ti^{4+}_{0.09}$	$Al_{0.43}Mg_{0.30}Fe^{2+}_{0.94}Fe^{3+}_{1.11}Ti^{4+}_{0.20}$
Z	$Al_{0.96}Mg_{2.00}Cr_{3.04}$	$Al_{5.53}Mg_{0.47}$	$Al_{5.18}Mg_{0.82}$	$Al_{4.15}Mg_{1.85}$
Name	vanadio-oxy-chromium-dravite [a]	oxy-foitite [b]	oxy-schorl [c]	bosiite [d]

Empirical structural formula for:
sample PR1973 (Bosi et al. 2014),
$(Na_{0.97}K_{0.02}Ca_{0.02})^{Y}(V^{3+}_{2.21}Cr^{3+}_{0.54}Fe^{3+}_{0.12}Mg_{0.11}Ti^{4+}_{0.01}Zn_{0.01})^{Z}(Cr^{3+}_{3.01}Al_{0.96}Mg_{2.03})[(Si_{5.99}Al_{0.03})O_{18}](BO_3)_3(OH_{2.87}O_{0.13})(O_{0.71}F_{0.29})$;
sample TM84a (Bosi et al. 2017d),
$(\square_{0.53}Na_{0.45}Ca_{0.01}K_{0.01})^{Y}(Al_{1.52}Fe^{3+}_{0.06}Fe^{2+}_{1.07}Mg_{0.25}Mn^{2+}_{0.05}Zn_{0.01}Ti^{4+}_{0.03})^{Z}(Al_{5.48}Fe^{3+}_{0.08}Mg_{0.36}Fe^{2+}_{0.08})[(Si_{5.89}Al_{0.11})O_{18}](BO_3)_3(OH)_3[O_{0.57}F_{0.04}(OH)_{0.39}]$;
sample PR85m (Bosi et al. 2017c),
$(Na_{0.69}K_{0.02}\square_{0.18}Ca_{0.11})^{Y}(Al_{1.23}Fe^{2+}_{0.90}Mg_{0.63}Fe^{3+}_{0.15}Ti^{4+}_{0.09})^{Z}(Al_{5.05}Mg_{0.89}Fe^{3+}_{0.06})[(Si_{5.99}Al_{0.01})O_{18}](BO_3)_3\ (OH)_3[O_{0.59}(OH)_{0.35}F_{0.06}]$;
sample drv18 (Cámara et al. 2002),
$(Na_{0.49}K_{0.01}Ca_{0.48})(Mg_{1.35}Fe^{2+}_{0.94}Fe^{3+}_{0.49}Ti_{0.20})(Al_{4.58}Fe^{3+}_{0.62}Mg_{0.80})[(Si_{5.99}Al_{0.01})O_{18}](BO_3)_{3.03}(OH)_3[(OH)_{0.18}F_{0.18}O_{0.64}]$.

[a] Ideally $NaV^{3+}_3(Mg_2Al_4)(Si_6O_{18})(BO_3)_3(OH)_3O$
[b] Ideally $\square(Fe^{2+}_2Al)Al_6(Si_6O_{18})(BO_3)_3(OH)_3O$
[c] Ideally $Na(Fe^{2+}_2Al)Al_6(Si_6O_{18})(BO_3)_3(OH)_3O$
[d] Ideally $NaFe^{3+}_3Al_6(Si_6O_{18})(BO_3)_3(OH)_3O$

This is a preprint, the final version is subject to change, of the American Mineralogist (MSA)
Cite as Authors (Year) Title. American Mineralogist, in press.
(DOI will not work until issue is live.) DOI: http://dx.doi.org/10.2138/am-2017-6289

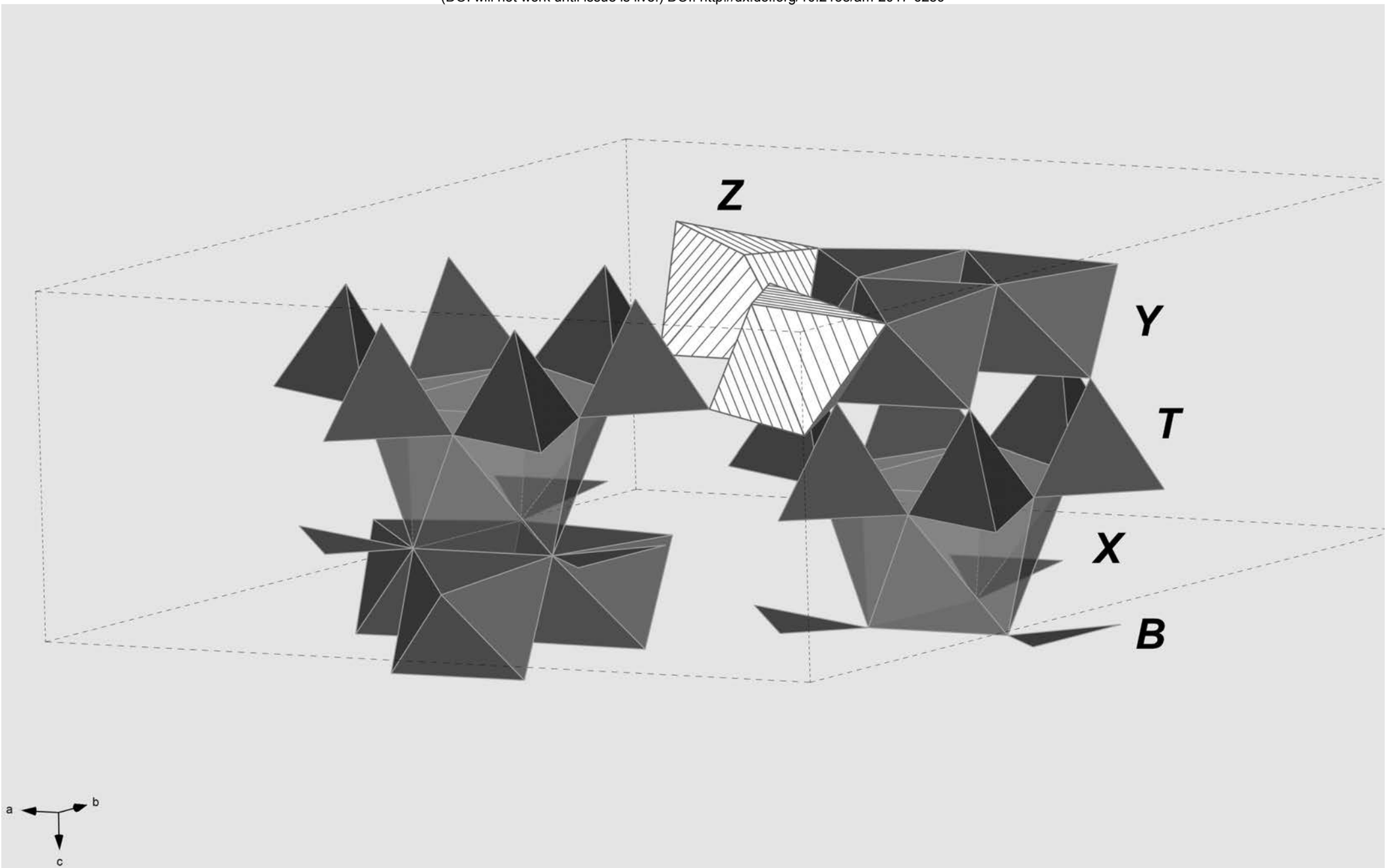

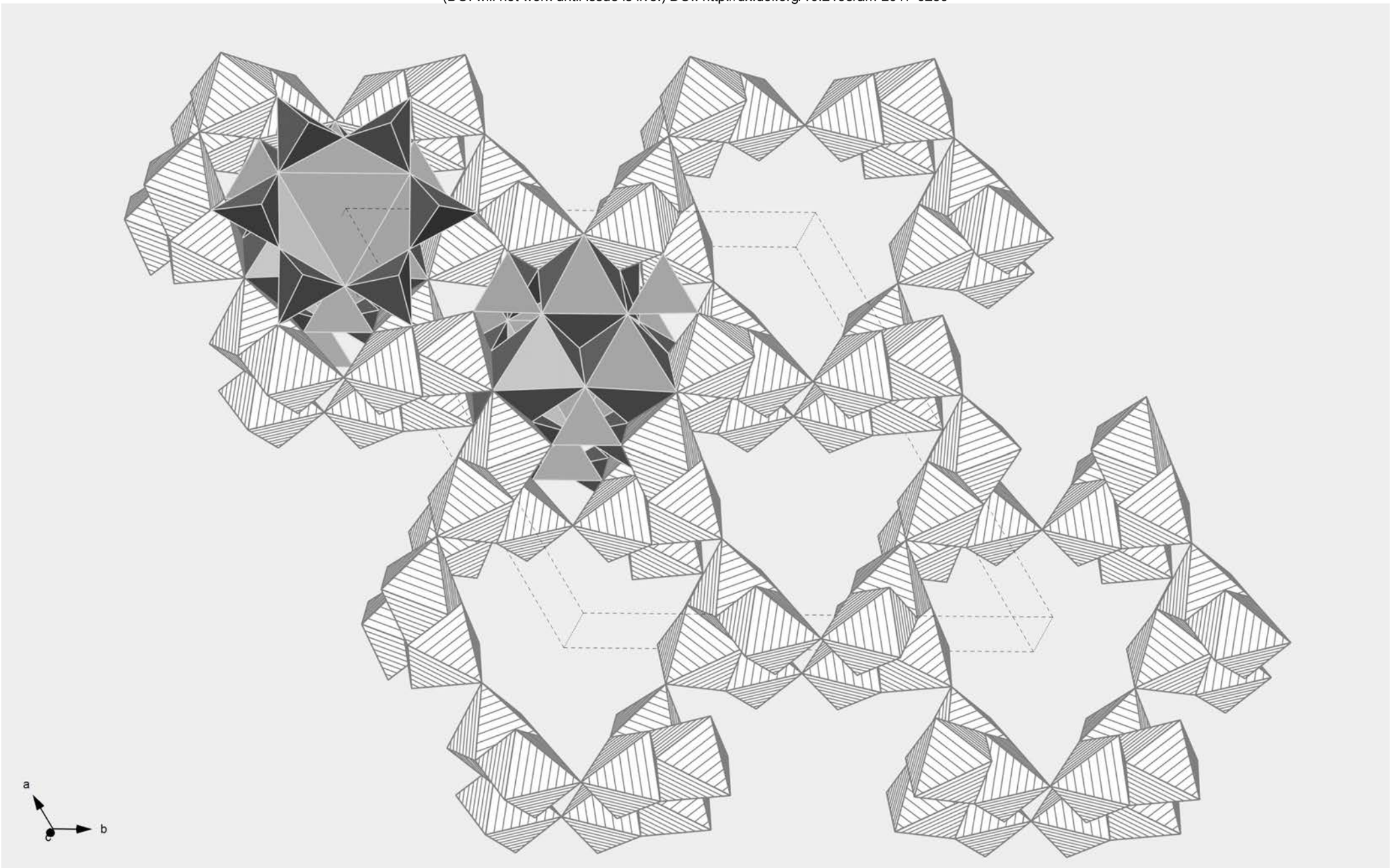

This is a preprint, the final version is subject to change, of the American Mineralogist (MSA)
Cite as Authors (Year) Title. American Mineralogist, in press.
(DOI will not work until issue is live.) DOI: http://dx.doi.org/10.2138/am-2017-6289

Figure 3

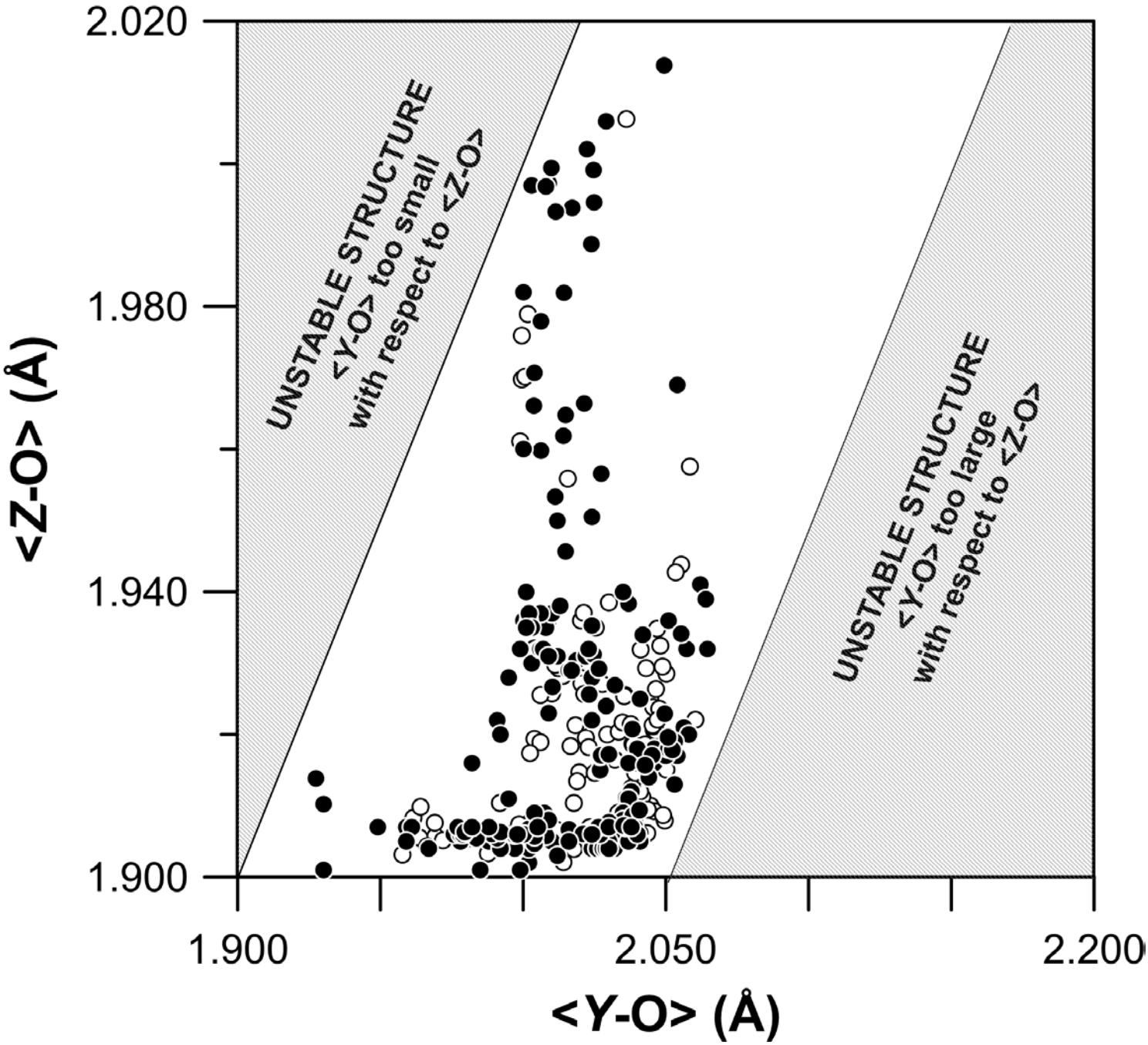

This is a preprint, the final version is subject to change, of the American Mineralogist (MSA)
Cite as Authors (Year) Title. American Mineralogist, in press.
(DOI will not work until issue is live.) DOI: http://dx.doi.org/10.2138/am-2017-6289

Figure 4

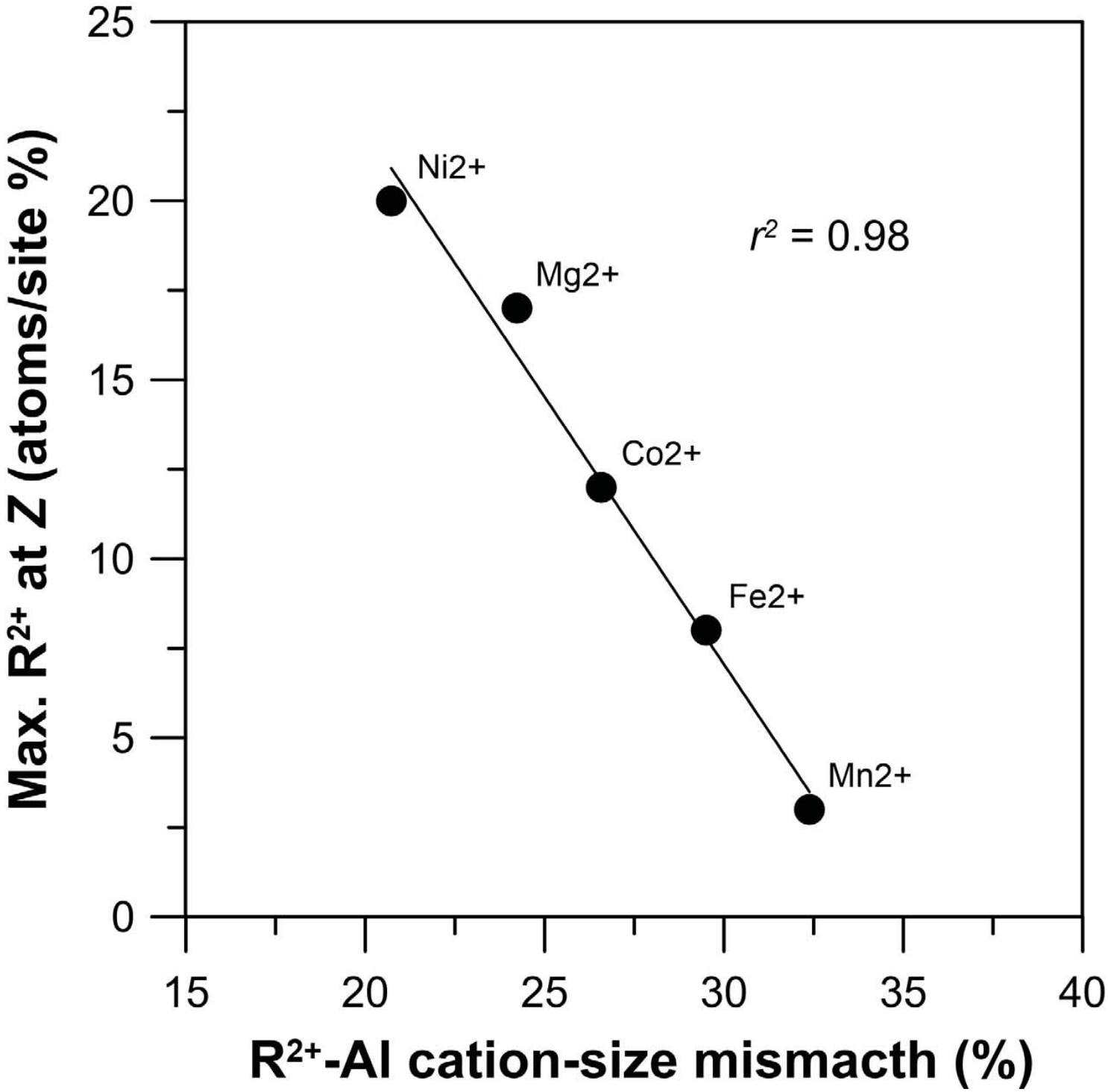

This is a preprint, the final version is subject to change, of the American Mineralogist (MSA)
Cite as Authors (Year) Title. American Mineralogist, in press.
(DOI will not work until issue is live.) DOI: http://dx.doi.org/10.2138/am-2017-6289

Figure 5